 doi:10.20944/preprints202202.0211.v1

Comparative analysis of the *pIgR* gene from the Antarctic teleost *Trematomus bernacchii* revealed distinctive features of cold adapted Notothenioidei

Alessia Ametrano[1], Simona Picchietti[2], Laura Guerra[2], Stefano Giacomelli[1], Umberto Oreste[1], Maria Rosaria Coscia[1,*]

[1] Institute of Biochemistry and Cell Biology, National Research Council of Italy, Via P. Castellino 111, 80131 Naples, Italy; alessia.ametrano@ibbc.cnr.it (A.A.); stefano77g@hotmail.it (S.G.); umberto.oreste@ibbc.cnr.it (U.O.); mariarosaria.coscia@ibbc.cnr.it (M.R.C)

[2] Department for Innovation in Biological, Agro-food and Forest Systems, University of Tuscia, Largo dell'Università, 01100 Viterbo, Italy; picchietti@unitus.it (S.P.); lauraguerra@unitus.it (L.G.)

* Correspondence: mariarosaria.coscia@ibbc.cnr.it; Tel: +0039 081 6132556 (M.R.C.)

Abstract: Previously, we identified and characterized the IgM and IgT classes in the Antarctic teleost *Trematomus bernacchii*, a species belonging to the Perciform suborder Notothenoidei. Herein we characterized the gene encoding the polymeric immunoglobulin receptor (pIgR) in the same species and compared it to pIgR of multiple teleost species belonging to five perciform suborders, including 11 Antarctic and one non-Antarctic (*Cottoperca gobio*) notothenioid species, the latter living in less cold periantarctic sea. Analysis of *T. bernacchii* pIgR cDNA unveiled multiple amino acid substitutions unique to Antarctic species, all introducing adaptive features, including N-glycosylation sequons. Interestingly, *C. gobio* shared most features with the other perciforms rather than with the cold adapted relatives. *T. bernacchii* pIgR transcripts were predominantly expressed in mucosal tissues, as indicated by q-PCR and *in situ* hybridization analysis. These results suggest that in cold adapted species pIgR preserved its fundamental role in mucosal immune defense, although remarkable gene structure modifications occurred.

Keywords: pIgR; gene structure; cold environment; gene expression; teleost immunity; adaptive evolution; mucosal tissues; genome alteration; Notothenioidei; IgV domains.

1. Introduction

The polymeric immunoglobulin receptor (pIgR) emerged early in evolution with teleost fish [1] and coevolved with mucosal Ig isotypes, ensuring a mucosal protection [2]. It has a conserved structure, consisting of an extracellular region composed of varying numbers of IgV domains, increasing across the evolutionary scale [3], a transmembrane region and a cytoplasmic tail [4]. In mammals, pIgR has five IgV domains (D1-D5), except for the bovine and rabbit IgRs having three (D1, D4, and D5) of the five domains, derived from alternative splicing [5, 6]. In birds, reptiles and amphibians, pIgR consists of four domains, corresponding to mammalian D1, D3, D4 and D5 [7-9]. The fish pIgR shows the simplest topology, based on comparative sequence analyses, comprising only two Ig-like domains, which are homologous to mammalian D1 and D5 [10]. Teleost pIgR is known to be expressed in

Preprints (www.preprints.org) | NOT PEER-REVIEWED | Posted: 17 February 2022 doi:10.20944/preprints202202.0211.v1

mucosa-associated lymphoid tissues, e.g., intestine, gills, skin, buccal and pharyngeal cavity, and olfactory system [11]. pIgR has been shown to bind both IgM and IgT, although the exact Ig-binding sites of pIgR has not yet been clarified, given that polymeric Igs (pIgs) are devoid of J chain, contrary to cartilaginous fish in which the J chain has been identified [12].

Over recent years, great attention has been paid to the function of fish pIgR, while studies aimed at examining its gene structure are still limited. Full-length transcripts from the *pIgR* gene were characterized in various teleost species belonging to different orders [11], and the binding sites of cytokine-inducible regulatory elements, well known in mammals, were also predicted and considered as potential regulators of the transcription of *pIgR* in teleost fish [13-15].

At present, no data are available on pIgR from teleost species living under extreme conditions, such as Notothenioidei (Perciform suborder) that represent the prevalent component of the Antarctic fish fauna. During their evolutionary history, Nototheniodei have undergone extraordinary challenges to finally adapt to the constantly cold marine environment of Antarctica. The Antarctic notothenioid families have been proposed as a superfamily, named Cryonotethenioidea [16], to be distinguished from the non-Antarctic families that are considered the most phyletically basal branch, since having remained in periantarctic seawaters, under temperate conditions [17, 18]. This taxonomic group has long been considered an attractive model to study biochemical, physiological and morphological adaptations, although poorly investigated at a molecular level. In previous studies, we investigated the genes encoding IgM and IgT isotypes in several cold-adapted and temperate notothenioid species [19-21] and highlighted the first evidence for a possible hepato-biliary transport of Ig in the Antarctic species *Trematomus bernacchii* [22].

The most recent advances in collecting omics data from notothenioid fish provided a source of fundamental information about molecular and genetic features, allowing to carry out also evolutionary studies on notothenioids in comparison with other perciform species. Thus, our main goal for this study was to investigate the specificities of the *pIgR* gene related to the evolutionary adaptation, through a comparative analysis, based on the transcriptomes publicly available for *T. bernacchii* and for 11 Antarctic species belonging to the same suborder as *T. bernacchii* (Notothenoidei). In particular, we extended the analysis to *Trematomus loenbergii*, *Dissostichus eleginoides*, *Dissostichus mawsoni, Notothenia coriiceps* (family Nototheniidae), *Harpagifer antarcticus* (family Harpagiferidae), *Gymnodraco acuticeps* (family Bathydraconidae), *Pseudochaenichthys georgianus, Chaenocephalus aceratus, Chionodraco myersi* and *Chionodraco hamatus* (family Channichthyidae), all adapted to live in the extreme environment of Antarctica. Moreover, another notothenioid species, *Cottoperca gobio*, belonging to the family Bovichtidae, the ancestral notothenioid family living in the more temperate periantarctic seawaters, was added for comparison. Additionally, 26 perciform species, belonging to five different families, were included for comparative analysis. Finally, the expression of *T. bernachii pIgR* gene was evaluated through q-PCR and *in situ* hybridization (ISH) first allowed transcript localization.

Preprints (www.preprints.org) | NOT PEER-REVIEWED | Posted: 17 February 2022 doi:10.20944/preprints202202.0211.v1

Taken together, these findings underline several peculiar features that may be considered as the hallmark of cold pIgRs and underpin the primary role of pIgR in mucosal immune response and host protection in a cold adapted teleost species.

2. Results

2.1 Analysis of T. bernacchii pIgR cDNA

Initially, a partial cDNA sequence of the pIgR was obtained from total RNA extracted from the spleen of a *T. bernacchii* specimen as described in the Methods section. The primers used for PCR experiments were designed on the nucleotide sequences encompassing the *pIgR* D1-D2 domains from *Epinephelus coioides*. The amplicon obtained of 529 nt was cloned and sequenced. Subsequently, to extend the 5′ end of cDNA, a 5′ RACE was performed by using the gene specific primer pIGR1Rev, designed at the beginning of the D1 domain; the antisense primer pIGRIIr, designed in the middle of the D2 domain, was used for the nested PCR amplification. The amplicon obtained (235 nt) was cloned and sequenced.

To complete the sequence at the 3′ end of the *pIgR* transcript, a 3′ RACE was carried out by using pIGR1Fwd as sense specific primer. To verify the correct amplification, a nested PCR reaction was performed, using pIGRII as sense primer. The amplicon obtained (650 nt) was cloned and sequenced.

The full-length cDNA sequence encoding *T. bernacchii* pIgR consisted of 1414 nt, including a 5' UTR (38 nt) and a 3' UTR (359 nt) (Figure 1). Two polyadenylation signals were identified, one canonical, at position 1387, and a second one, non-canonical, at position 1395 (Figure 1).

Thirty positions were polymorphic because found different from those in the transcript variants. Five carried non-synonymous substitutions. Interestingly, a fairly critical mutation was identified in the fourth position of the canonical polyadenylation signal, which abolishes its usage. In this circumstance, the non-canonical poly(A)-site more likely becomes functional.

The functional protein domains were identified in the deduced amino acid sequence by using the bioinformatics tools SignalP, Prosite, TMpred. Following a 21-aa long signal peptide, two immunoglobulin domains, D1 and D2, consisting of 108 and 95 residues, respectively, were found, separated by a short linker sequence (Figure 1). The D1 and D2 domains were both identified as IgV domains, being the two conserved cysteine residues forming the intrachain disulfide bond spaced by 68 aa (D1) or 62 aa (D2), which is a distance greater than that found in IgC-and IgI- type domains. Furthermore, the presence of two additional cysteine residues, spaced by seven amino acid residues in both domains, is a typical feature of the IgV domains of pIgRs. It was noted that, while D1 is encoded by a single exon, the D2 nucleotide sequence comprises also one intron, which is an unusual feature for IgV domains. A 39-aa extracellular proximal domain (EMPD) sequence, with a high theoretical pI (11.0), rich in

Preprints (www.preprints.org) | NOT PEER-REVIEWED | Posted: 17 February 2022 doi:10.20944/preprints202202.0211.v1

prolines (17.9%), was preceding, at the carboxy-terminus of D2, the transmembrane domain (TM). The latter consisted of 20 residues and was characterized by a preponderance of leucine residues (30%) and by the presence of a cysteine residue, very infrequent in transmembrane proteins (Figure S1). The sequence ended with a 51-aa long basic cytoplasmic tail (Figure 1). The amino acid composition of *T. bernacchii* pIgR is reported in Table S1.

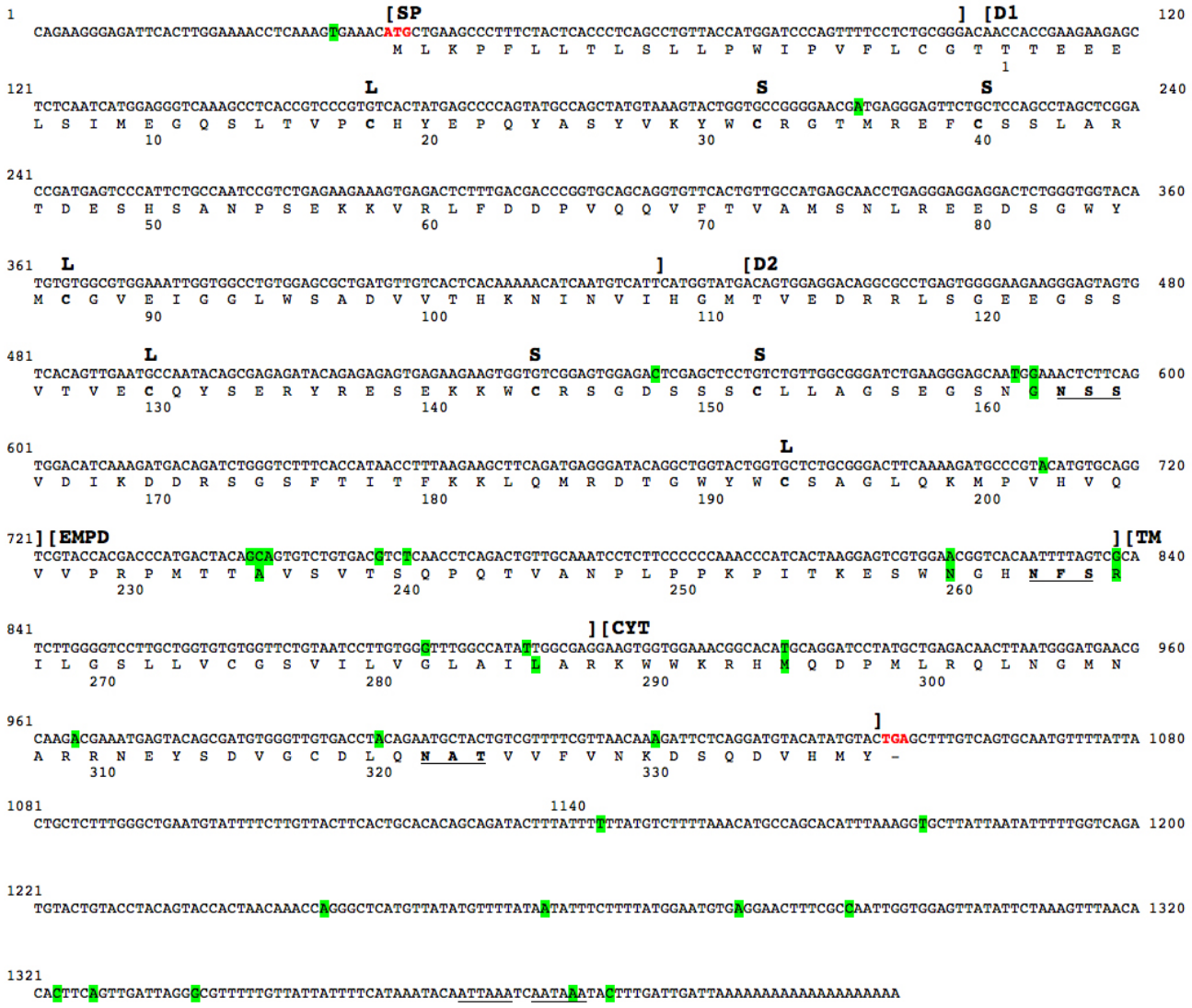

Figure 1. Nucleotide and deduced amino acid sequences of the gene encoding *T. bernacchii* pIgR. The start and the stop codons are given in bold red, the polyadenylation signals, located downstream of the stop codon, are underlined. The boundaries of the signal peptide (SP), the D1, D2 and EMPD domains, and the transmembrane (TM) and cytoplasmic (CYT) regions are indicated above the nucleotide sequence. Polymorphic sites are highlighted in green. Amino acid residues are reported in one-letter code below the nucleotide sequence. The large (L) and the small (S) loops are indicated above codons for the cysteine residues forming them. N-glycosylation sites defined by the NXS/T sequons are bold and underlined. Numbering of nucleotides and of amino acids residues is reported above and below each sequence, respectively.

Preprints (www.preprints.org) | NOT PEER-REVIEWED | Posted: 17 February 2022 doi:10.20944/preprints202202.0211.v1

As previously shown by the AT content analysis of notothenioid *IgT* genes [21], most interestingly, a remarkably high AT content of *pIgR* exons was shared within Antarctic species, reaching a peak (55.8 %) in the family Nototheniidae, which comprises *T. bernacchii* and *Dissostichus eleginoides* (Figure 2). This finding reflects a peculiar feature neither shared with the non-Antarctic species *C. gobio*, their closest relative, nor with all the other Perciformes.

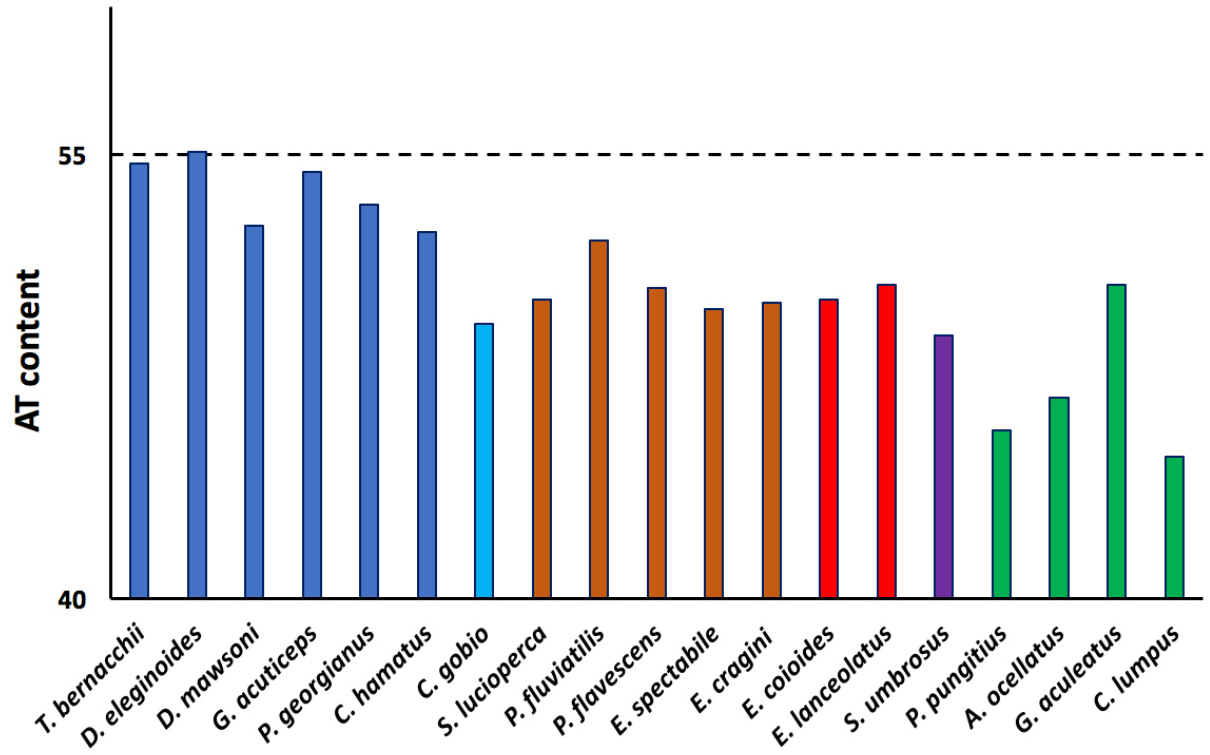

Figure 2. Percentage of AT content of the *pIgR* exons of Antarctic (blue bars) and in the non-Antarctic notothenioid species *C. gobio* (light blue bar) compared to representative species of the temperate perciform suborders Percoidei (brown bars), Serranoidei (red bars), Scorpaenoidei (purple bar), Cottoidei (green bars).

2.2 Analysis of T. bernacchii pIgR deduced amino acid sequence

In order to identify adaptive characteristics unique to notothenioid pIgR sequences, we extended our analysis to other notothenioid species and to representatives of the five perciform suborders, on the basis of the available data (see Material and Methods Section 4.1). Some conserved motifs, previosly identified in other fish and suggested to help stabilize the secondary structure of pIgR [14], were also found in D1 (CWDC, KYWC and DxGxYxC motifs) and D2 of *T. bernacchii* pIgR (KxWC and DxGWYWC) (Figure 3).

Preprints (www.preprints.org) | NOT PEER-REVIEWED | Posted: 17 February 2022 doi:10.20944/preprints202202.0211.v1

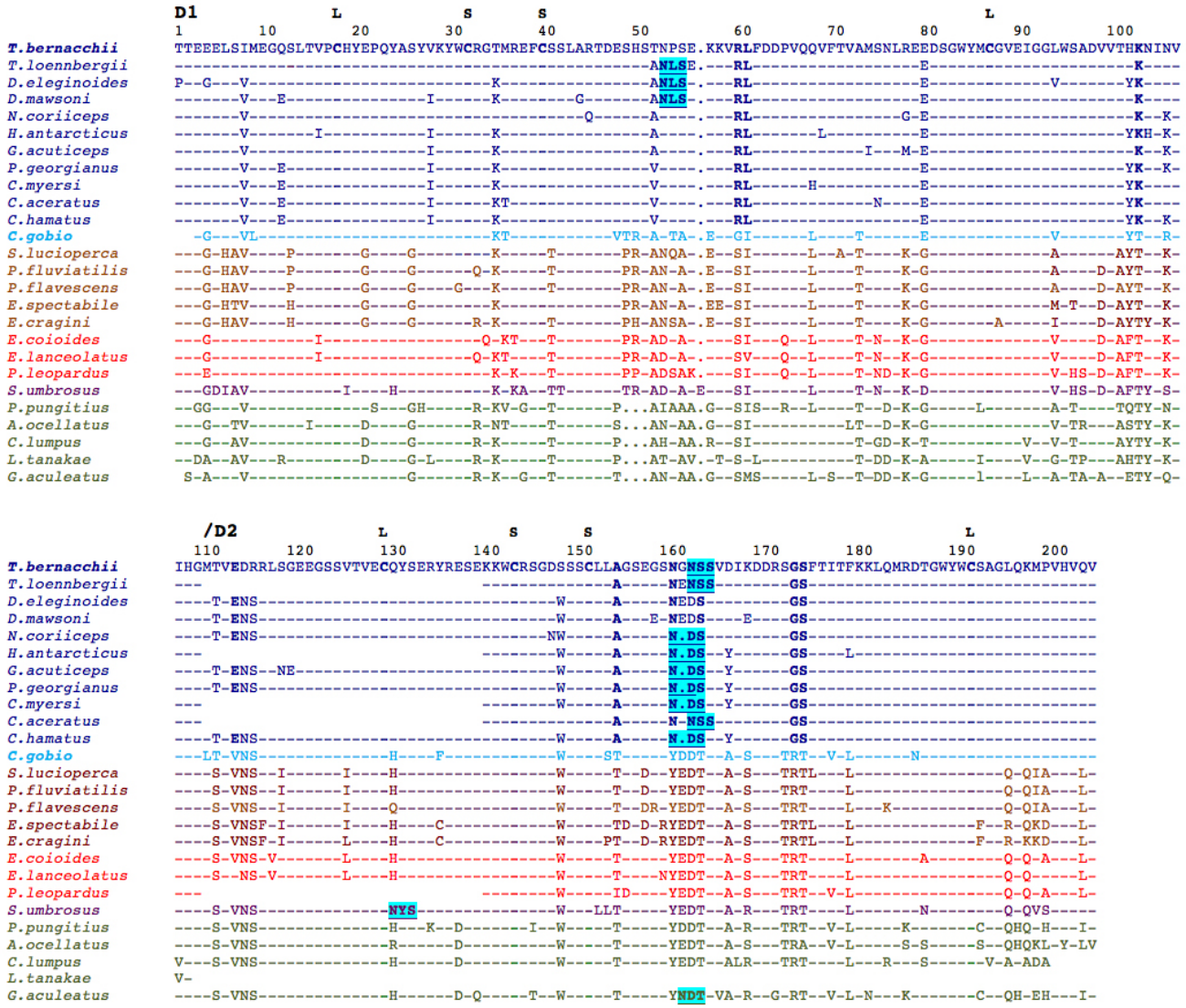

Figure 3. Multiple amino acid sequence alignment of pIgR D1-D2 domains from Notothenioidei (in blue; *T. bernacchii* in bold blue and *C. gobio* in bold light blue) and other species of the perciform suborders Percoidei (in brown), Serranoidei (in red), Scorpaenoidei (in purple), and Cottoidei (in green). Notothenioid specific residues are reported in bold. The highly conserved cysteine and tryptophan residues characteristic of the immunoglobulin fold are in bold. The large (L) and the small (S) loops are indicated above the cysteine residues forming them. Putative N-glycosylation sites are underlined and highlighted in cyan. Amino acid residues that are identical to those shown in the sequence of *T. bernacchii* are indicated by dashes. Gaps are indicated by dots. The complete alignment is shown in Figure S2.

Nineteen amino acid positions were found to be specific for Antarctic pIgRs, as present in all Antarctic sequences, but absent in all sequences from the other species analyzed, as well as in the non-Antarctic notothenioid *C. gobio* (Figure S2). Ten of them were present in the secretory component; three positions (R60, L61 and K103) were localized in the D1 domain, six in D2 (E114, A155, N161, S164, G174 and S175) (Figure 3), one in the EMPD, three in the TM domain and six in the cytoplasmic tail (Figure S2). In addition, it is worth of remark that five out of ten notothenioid-specific residues, which are present in the extracellular portion of the receptor, introduce or abolish an electrostatic charge; N161 and S164 are convergent substitutions since introducing a glycosylation sequon

Preprints (www.preprints.org) | NOT PEER-REVIEWED | Posted: 17 February 2022 doi:10.20944/preprints202202.0211.v1

NXS/T (being X different from P). Two additional residues (E79 and T112) were shared by Antarctic and non-Antarctic nothotenioid species but they were absent in the other perciform suborders (Figure 3).

Glycosylation was found to be another distictive feature of the notothenioid pIgR. Up to four N-glycosylation sequons were found in Antarctic fish compared to the other perciform species, which showed no sequons at all, except for *Sebastes umbrosus* and *G. aculeatus*, harboring just one (Figure 4). Interestingly, the site in D2, which is present in 9 out of 12 sequences, is alternately located at two asparagines spaced by a single residue (Figure 3).

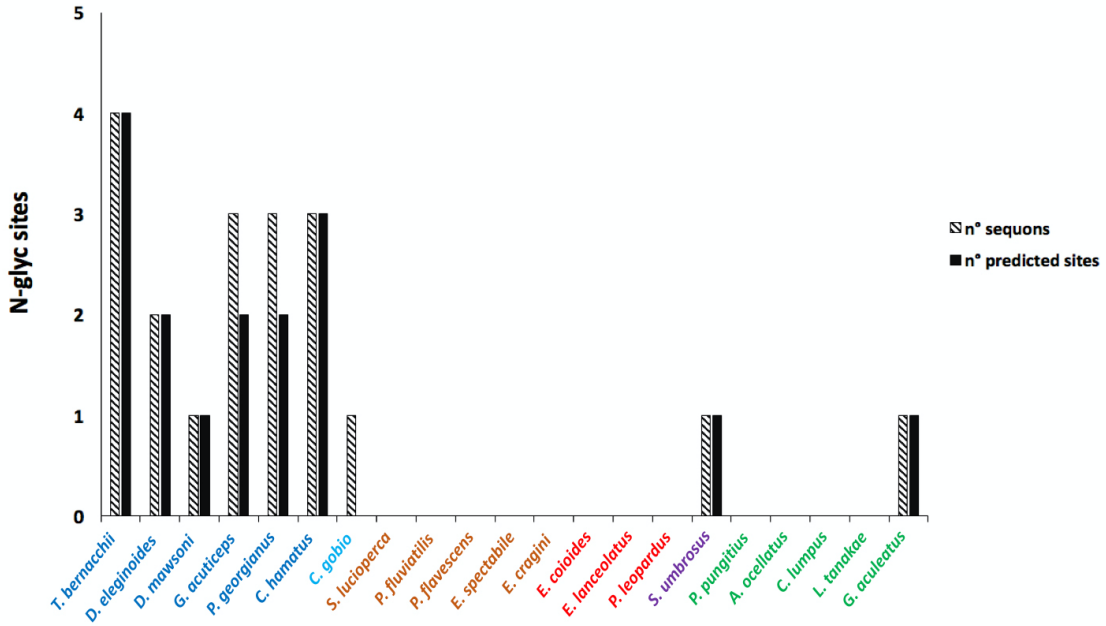

Figure 4. Distribution of potential N-glycosylation sequons (diagonal black bars) and glycosylated sequons (black bars) in the pIgR of Antarctic (in blue) and non-Antarctic (in light blue) notothenioid species, compared to representative species of the temperate perciform suborder Percoidei (in brown), Serranoidei (in red), Scorpaenoidei (in purple), Cottoidei (in green).

Interestingly, all the sequons identified were predicted to be glycosylated in most Antarctic species, except two out of three in *G. acuticeps* and *P. georgianus*. Of the four notothenioid N-glycosylation sites, one occurs in each of the D1 and D2 domains, one at the boundary between the TM region and the extracellular portion, another one is in the cytoplasmic tail (Figure S2). The distance tree generated from the multiple alignment clearly confirms phylogenetic relationships among the species analyzed (Figure 5).

Preprints (www.preprints.org) | NOT PEER-REVIEWED | Posted: 17 February 2022 doi:10.20944/preprints202202.0211.v1

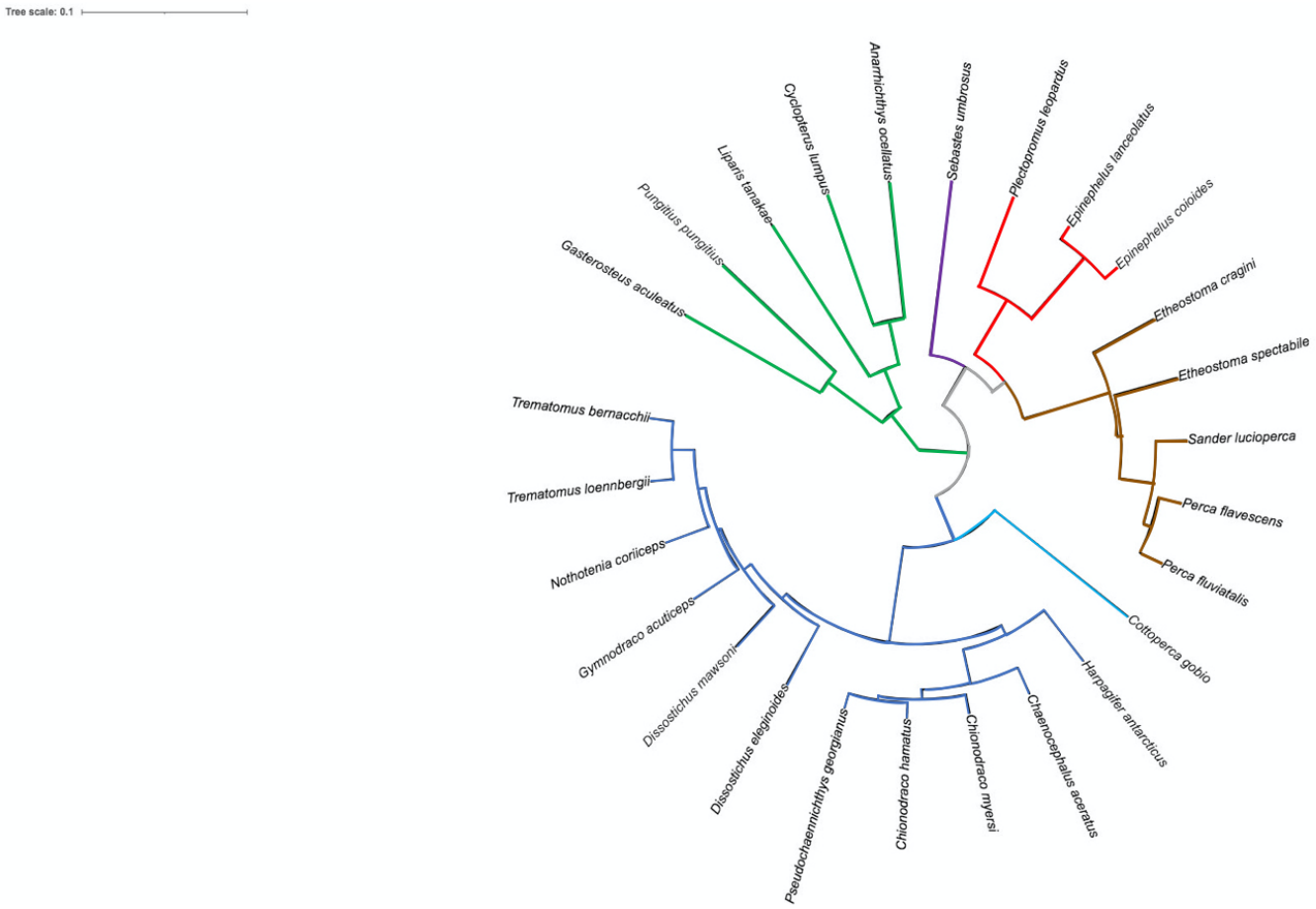

Figure 5. Distance tree of the pIgR D1 domain from teleost species belonging to the perciform suborders Notothenioidei (Antarctic species blue lines; non-Antarctic species light blue line), Percoidei (brown lines), Serranoidei (red lines), Scorpaenoidei (purple lines), and Cottoidei (green lines). The tree was generated by the Clustal Omega tool. The sequences used are as in Figure 3.

2.3 Structural analysis of T. bernacchii pIgR

We constructed a molecular model of the ectodomain of *T. bernacchii* pIgR. It consists of two tandem IgV domains, D1 and D2, whose axes diverge of about 120°. Differently from other IgV domains, a disulfide bridge connects C and C′ strands in both D1 and D2 domains. The regions that are defined as complementary determining regions (CDRs) in the antibody VH and VL domains were recognized in the D1 domain (Figure 6). D1 CDR loops are more extended, while the structure of D2 appears more compact and contains an additional C′′ strand. Minor structural differences between trout, selected as template strcuture, and *T. bernacchii* are related to the size of D1 CDR2, which is longer in *T. bernacchii* (Figure 6).

Preprints (www.preprints.org) | NOT PEER-REVIEWED | Posted: 17 February 2022 doi:10.20944/preprints202202.0211.v1

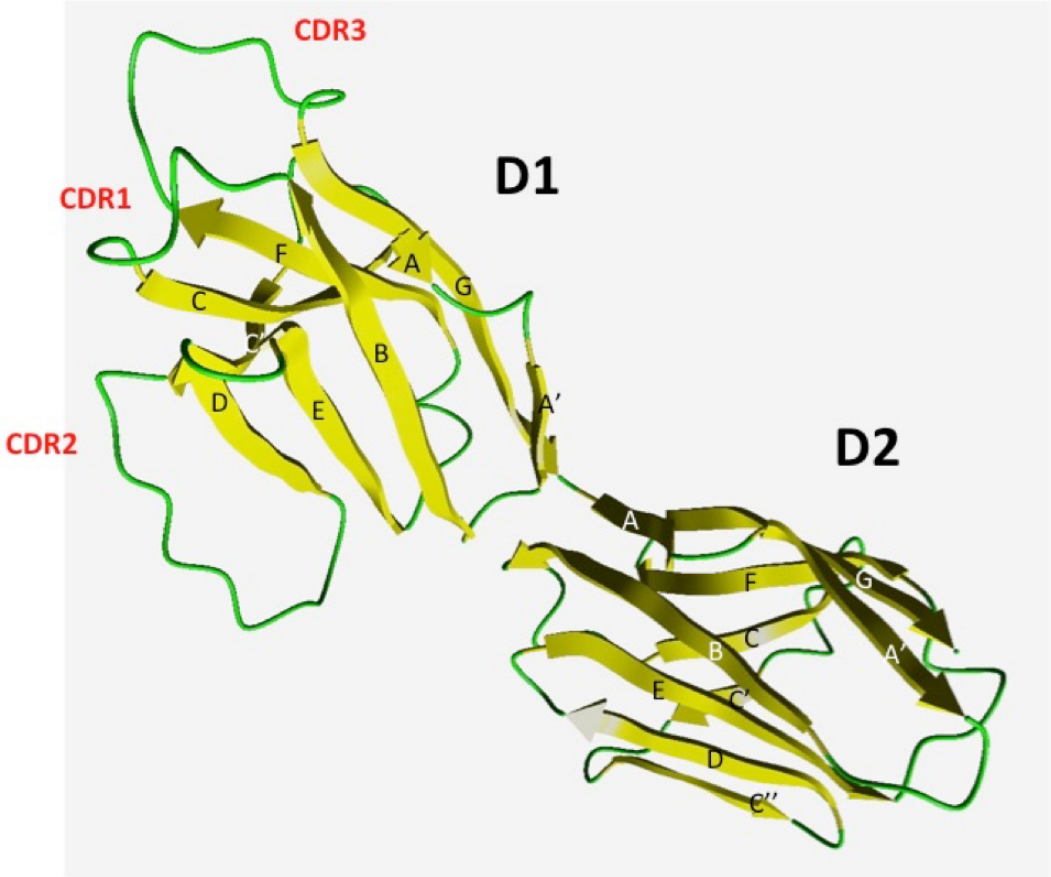

Figure 6. Ribbon representation of the molecular model of *T. bernacchii* pIgR extracellular region. The β-strands are labeled with uppercase letters. Loops that correspond to the three Complementary Determining Regions in the D1 domain are labeled (CDR) and colored (green).

The N-glycosylation sites of D2 were found to be exposed to the solvent (Figure S3), suggesting a role of the attached carbohydrate moiety. Notably, all substitutions introducing electrostatic charges in notothenioids were also found to expose the side chain to the solvent as well as the glycosylated N161, suggesting that the solubility of the molecule increases at the very low temperature of the Antarctic seawater. The position of the Antarctic species-specific charged residues R60, K103, E114 and N161 is shown in Figure S3.

2.4 Basal expression analysis of pIgR transcripts in T. bernacchii mucosal tissues and lymphoid organs

To gain some insights into the constitutive expression of pIgR in a cold adapted teleost, a relative mRNA expression pattern of the gene was determined by q-PCR in mucosal tissues and lymphoid organs of *T. bernacchii*. As shown in Figure 7, *pIgR* transcripts were expressed in all the tested tissues, with the highest abundance detected in gills and the lowest in muscle, as expected. Higher levels were also found in the intestinal segments. In particular, the mRNA levels in the middle intestine were 2.7-fold (adjusted $p < 0.01$) and 3.9-fold (adjusted $p < 0.05$) lower than those in the anterior and posterior ones, respectively. No statistically significant transcriptional

Preprints (www.preprints.org) | NOT PEER-REVIEWED | Posted: 17 February 2022 doi:10.20944/preprints202202.0211.v1

differences were found between the anterior and posterior segments. A moderate *pIgR* expression was detected in liver and head kidney, being the former 3.9-fold and the latter 10-fold lower than gills (adjusted $p < 0.001$). These findings are consistent with the predominant role of pIgR in mucosal compartments.

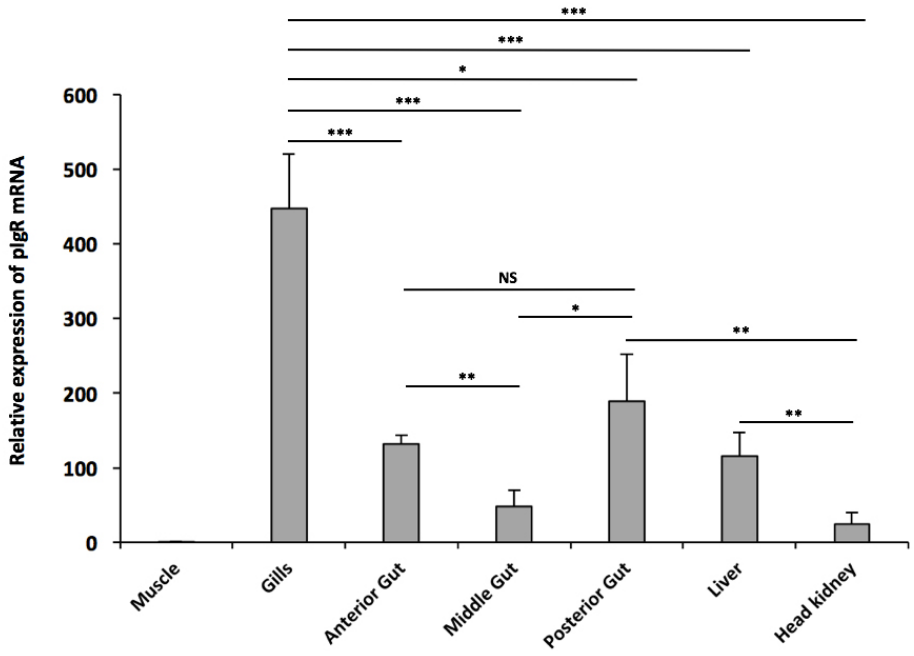

Figure 7. Relative expression levels of *pIgR* in different tissues from *T. bernacchii*. Data from three independent experiments are presented as mean gene expression relative to the housekeeping β-actin (± SD). The muscle tissue was used as negative control. Levels of transcription were evaluated by q-PCR in duplicates using three *T. bernacchii* specimens. *p < 0.05**;** **p <0.01; ***p < 0.001; NS, not significant (two-tailed Student's t test with Bonferroni correction).

2.5 pIgR expressing cells in T. bernacchii intestinal and hepatic tissues

To identify pIgR-producing cells in *T. bernacchii* tissues we performed ISH analysis with anti-sense and sense RNA DIG labelled probes. Given the results obtained by q-PCR, we paid a special attention to the gut-liver communication axis. The posterior intestine, that displayed higher *pIgR* expression levels (Figure 7), was lined by a simple columnar epithelium of polarized cells (enterocytes) (Figure 8a-d). In this species, all the enterocytes were *pIgR*-expressing cells (Figure 8a-c). In particular, the highest staining intensity was detected around the nucleus and on the enterocyte basolateral surface, that face the basement membrane (Figure 8b). The apical surface of most epithelial cells did not display any staining. Scattered cells, localized both in the epithelium (Figure 8b) and the underlying lamina propria, were stained (Figure 8c). Moreover, the staining with the anti-sense probe (Figure 8e) revealed a strong signal throughout the liver. Notably, the expression of the *pIgR* gene was mainly detected around

Preprints (www.preprints.org) | NOT PEER-REVIEWED | Posted: 17 February 2022 doi:10.20944/preprints202202.0211.v1

the nucleus of most hepatocytes. ISH with pIgR sense probe did not result in any staining both in the posterior intestine and liver, as expected (Figure 8 d-f).

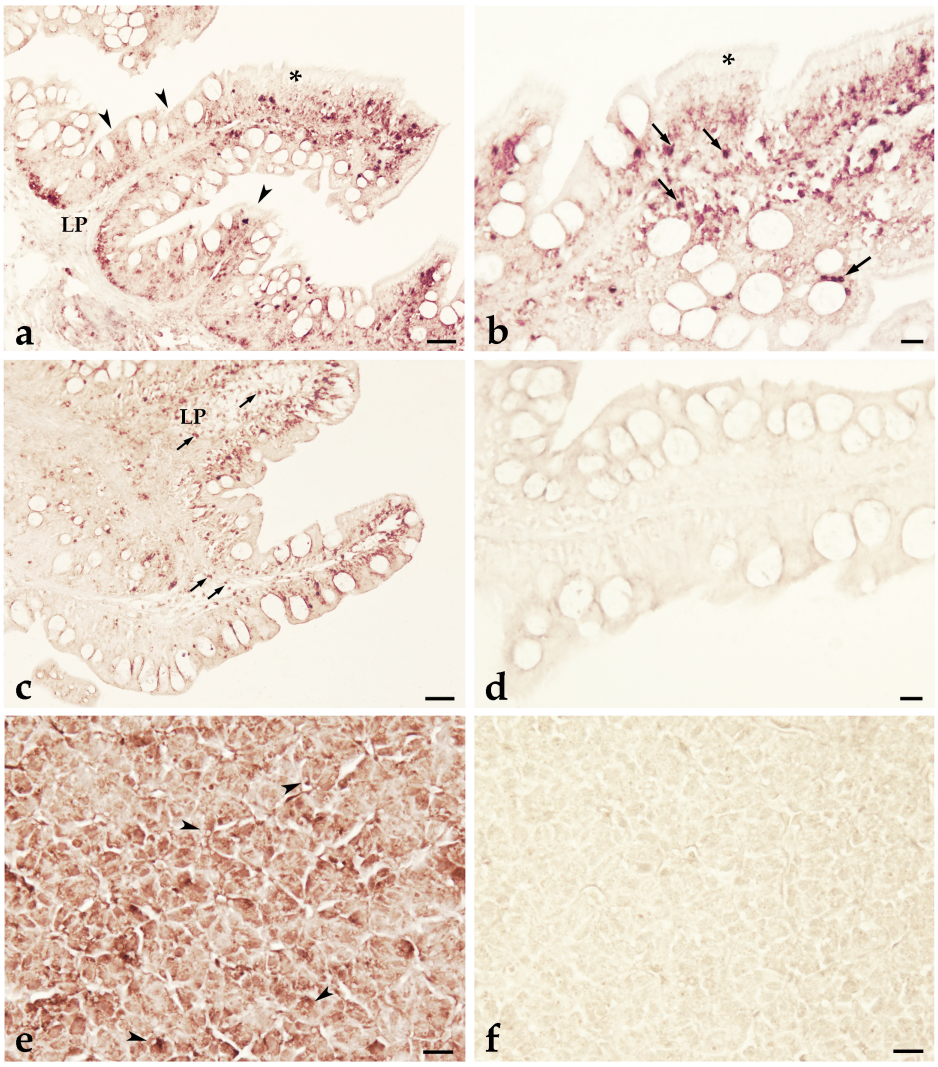

Figure 8. ISH of *T. bernacchii* pIgR. pIgR-expressing cells were detected in *T. bernacchii* (posterior) gut (a-c) and liver (e) using an antisense probe. No signals were detected in either intestine (d) or liver with a sense probe (f). Stained enterocytes and liver epithelial cells are shown by arrowheads. Scattered cells containing pIgR transcripts are mainly in the epithelium and in the lamina propria (arrows). LP, lamina propria; * apical surface of enterocytes. Scale bars: 20 μm.

Discussion

The pIgR plays a crucial role in mammalian immune responses, since it ensures multifaceted immune functions [15, 23]. The pIgR has been studied in multiple teleost fish species, highlighting similarities and differences in its structure, as reviewed by Kortum et al. [15]. However, data about the teleost pIgR functions are very limited and mainly referred to the transport of pIgs across the mucosal epithelial cells [2, 11, 13-15]. Also, the *pIgR* gene locus

Preprints (www.preprints.org) | NOT PEER-REVIEWED | Posted: 17 February 2022 doi:10.20944/preprints202202.0211.v1

organization still remains poorly investigated. The *pIgR* gene has been identified so far in zebrafish as a single copy, along with a wide multigene family that comprises *pIgR-like* (*pIgRL*) genes, differentially expressed in lymphoid and myeloid cells [15]. As well, a BLAST search of the *Takifugu rubripres* genome database allowed identification of a *pIgR* homologous gene [24].

To expand the current knowledge in this field, we isolated and characterized, for the first time, the *pIgR* gene in the cold adapted teleost species *T. bernacchii*.

In the present study, we found that *T. bernacchii* pIgR consisted of two immunoglobulin domains, D1 and D2, separated by a short linker sequence, EMPD sequence, rich in prolines, the TM domain. In contrast to human pIgRs, which are extensively glycosylated, fish pIgRs show limited or even no glycosylation sites. These data raise the question whether the N-glycosylation of pIgR is necessary for its function. This is an interesting issue that became even more relevant when we highlighted the presence of up to four N-glycosilation sites exclusively in pIgRs from Antarctic species. In addition, all sites were predicted to be glycosylated, thus appearing as a distinctive feature of cold. In particular, the asparagine residue of the glycosylation sequon present in the extracellular portion of *T. bernacchii* pIgR was found exposed to the solvent in the molecular model we built, indicating the carbohydrate availability for binding. As a general role, carbohydrates are involved in protein folding, stability and protection from proteolytic attacks. Glycosylation can also modulate a correct balance between protein solubility and structural flexibility. This role can be viewed as a special adaptive response to cold environment, such as in the case of Antarctic fish IgT and IgM, found to be highly glycosylated [21, 25]. A further element that indicates an increase in solubility is related to the greater surface electrostatic charge. In fact, we noticed that some amino acid residues, specific for the cold-adapted species, introduced electrostatic charges located on the surface of our molecular model. These findings underlined several peculiar features that may be considered as the hallmark of cold pIgRs.

Despite the expression of the *pIgR* gene still needs further analysis, a single transcript of this gene is usually found in most fishes. However, in *Ctenopharyngodon idella*, seven pIgR splicing transcripts were identified, a full-length and six truncated variants, two generated by exon skipping and the other four having different motif arragements at the 3' end [26]. Furthermore, we analyzed *pIgR* expression in mucosal tissues and lymphoid organs, including the anterior, middle and posterior intestine, gills and head kidney.*T. bernacchi pIgR* transcripts were predominately expressed in the mucosal tissues, showing similar expression patterns to those of other teleosts species [10, 15, 24, 27, 28, 29]. The highest pIgR level detected in the gills is one of the most interesting aspects. Considering that gills represent one of the first lines of defence in teleosts, it will be challenging to assess whether the *pIgR* gene expression is upregulated in a tissue-specific manner in *T. bernachii*.

It is well known that in vertebrate genomes CGIs are involved in transcriptional regulation [30]. Varriale and Bernardi [31] reported an increase of CGIs and DNA methylation levels in Antarctic fishes, more likely being

 doi:10.20944/preprints202202.0211.v1

accompanied by the progressive cooling of Antarctic seawaters. However, the nature of regulatory elements and the mechanisms underlying transcription at low temperature are still little known and deserve further studies. Studies on regulation of the pIgR in response to pathogens, which are naturally occurring in the cold adapted fish investigated. e.g., the well documented nematode parasite infection [32, 33]. In other teleost species, high *pIgR* expression was found in gills after induced bacterial infection [11, 14].

Additionally, the pIgR mRNA had higher expression in the posterior intestine than in the middle segment and did not differ from the anterior segment. These results, in line with the findings collected from other teleost fish [29, 32], further confirmed that the posterior intestine plays an important role for the mucosal immune response and host defence.

High staining intensity was found through ISH in the cytoplasm of the enterocytes, suggesting that *T. bernacchii* pIgR mediates transepithelial transcytosis, as described in mammals [23].

Interestingly, scattered pIgR-expressing cells were also detected in the mucosa, as previously observed in *Cyprinus carpio* [48]. However, currently, there are not yet any markers to provide evidence on nature of these pIgR-expressing cells, although the staining may suggest an additional role played by pIgR molecules in teleost fish. In mammals, pIgR ensures multifaceted immune functions such as i) improving pIg stability, ii) protection of secretory Ig from proteolytic degradation, iii) exclusion of pathogens from mucosal surface, iv) intracellular neutralization of invading pathogens, v) removal of pathogen-secretory Ig complexes from infected tissues, and vi) nonspecific microbial scavenger function of free secretory component (SC) [23]. Data about these functions of pIgR in teleost mucosal immunity are very limited, although new findings provided direct evidence for pIgR-mediated immune excretion of IgM–antigen complexes in *Paralichthys olivaceus* [34].

Moreover, we considered the liver to expand the current knowledge about the *pIgR* expression and pIgR-mediated transport of SIgs in teleost hepatocytes [22, 35, 36]. The results obtained by q-PCR demonstrated that *pIgR* was expressed in *T. bernacchii* liver, and ISH demonstrated that the transcripts were localized around the nucleus of the hepatocytes. In this species IgM-immunoreactivity was detected in the perisinusoidal cells, bile canaliculi, pre-ductules and in the intraluminal mucus of the anterior intestine [22]. Taken together, the data strongly substantiate that *T. bernacchii* IgM may be transported via pIgR across the hepatocytes to be secreted into the bile and subsequent into the gut. This implies the putative formation of a receptor-Ig complex, as is the case in mammals [35, 36]. Numerous observations indicated that teleost pIgR binds IgM [24, 29, 37] and IgT [38, 39], while it remains to be elucidated whether this can occur for IgD. We consider that to improve the current understanding of *T. bernacchi* pIgR/SIg system and reveal the specific mechanisms of intracellular Ig transport, it will be necessary to rely on the availability of specific markers and adopt novel technologies from the field of molecular cell biology. Addressing these and other future studies will aid in further dissecting the complex roles of pIgR in mucosal immune defence of teleost fish.

Preprints (www.preprints.org) | NOT PEER-REVIEWED | Posted: 17 February 2022 doi:10.20944/preprints202202.0211.v1

In conclusion, our findings highlighted several peculiar features acquired by cold adapted pIgR and underpinned its pivotal role played in mucosal immune defence. The gene information gained in the present study will be useful for comparative and functional analyses, contributing to advance the current knowledge of the *pIgR* gene in teleost fish.

4. Materials and Methods

4.1 Biological samples

Specimens of the species *Trematomus bernacchii* (family Nototheniidae) were caught in the Ross Sea, in the proximity of the Italian "Mario Zucchelli" Station at 74° 42'S, 164°07'E, during the XXV Italian Antarctic Expedition (2009-2010). The activity permit, released by Italian National Program for Antarctic Research (PNRA), was in agreement with the "Protocol on environmental protection to the Antarctic Treaty" Annex V. Tissues were collected and immediately frozen in liquid nitrogen.

4.2 Cloning of pIgR transcript

Total RNA was extracted, using SV Total RNA Isolation System kit (Promega), from 150 mg of head kidney collected from a *T. bernacchii* specimen, homogenized by Potter-Elvehjem glass-Teflon. RNA quality was assessed on a 2% agarose gel and by measuring A260/A280 ratio, the concentration by reading absorbance at 260 nm with a NanoDrop 1000 Spectrophotometer (Thermo Scientific). RNA was then subject to DNase I treatment (Thermo Scientific, #EN0521), in order to avoid DNA genomic contamination for downstream analysis. cDNA was obtained from 1 µg of total RNA using Maxima H Minus Reverse Transcriptase (Thermo Scientific, #EP0751). The oligonucleotides used as primers to perform the first round-PCR amplification, were designed on the nucleotide sequence coding for the D1-D2 domains of *E. coioides* pIgR (accession number FJ803367), available in the GenBank database. The target sequence was amplified in a final volume of 25 µl using 2 µl cDNA (20 ng), 1,25 µM of specific primers (1.0 µM), 0.5 µl of dNTP Mix (0.2 µM), 2.5 µl 10X DreamTaq Buffer, 0,5 µl (1 U) of DreamTaq DNA polymerase (Thermo Scientific, #EP0705), up to volume with H_2O, as follows: 95 °C for 3 min, 35 cycles of 95 °C (30 s), 60 °C (30 s), and 72 °C (1 min) with a final extension at 72 °C for 10 min. In order to improve the yield of the specific target amplification, the PCR product was then subject to a second amplification, following the same conditions as the primary PCR. Primers used in all the PCR experiments are shown in Table S2, which also reports the target domains (D1-D2) of pIgR for each primer. PCR products were analyzed on a 1.5% agarose gel, subsequently purified by NucleoSpin® Gel and PCR Clean-up (Macherey-Nagel) and finally cloned into pGEM®-T Easy Vector (Promega, #A1360). Positive clones were screened by the blue/white method and sequenced on both strands on an ABI PRISM 3100 automated sequencer at Eurofins Genomics Europe Sequencing GmbH (Jakob-Stadler-Platz 7, 78467 Konstanz, Germany).

Preprints (www.preprints.org) | NOT PEER-REVIEWED | Posted: 17 February 2022 doi:10.20944/preprints202202.0211.v1

Sequencing chromatogram was visualized using the program FinchTV (version 1.3.0). The nucleotide sequence obtained was verified by sequence similarity searches against the GenBank database, using the BLAST program.

4.3 3′ and 5′ Rapid Amplification of cDNA Ends (RACE)

In order to complete 3′ cDNA region of *T. bernacchii pIgR*, 3′ Rapid Amplification of cDNA Ends (3′RACE) was performed using a commercial kit (Invitrogen™) according to manufacturer's instructions. First-strand cDNA was synthesized as described above, using AP as specific primer. PCR amplification was then carried out with pIGR1Fw as sense primer and AUAP as antisense primer. Subsequently a nested PCR was performed with pIGRII as sense primer and AUAP as antisense primer (Table S4). The amplification was performed as follows: 95 °C for 5 min, 40 cycles of 95 °C (30 s), 55 °C (30 s) and 72 °C (1 min) with a final extension at 72 °C for 15 min. 5′ Rapid Amplification of cDNA Ends (5′ RACE) was carried out on *T. bernacchii pIgR* cDNA using 5′ RACE System for Rapid Amplification of cDNA Ends version 2.0 (Invitrogen™), following the manufacturer's instructions. First-stranded cDNA was synthesized using an antisense specific primer pIGR1Rev. Subsequent PCR amplification was performed with pIGR1Rev and Oligo d(T)-anchor primer (AAP), supplied by the kit as sense primer. A nested PCR was performed with pIGRIIr and AAP. The amplification was performed as follows: 95 °C for 3 min, 40 cycles of 95 °C (30 s), 60 °C (30 s), 72 °C (1.30 min) with a final extension at 72 °C for 10 min.

3′ and 5′ RACE products were cloned and sequenced as described above.

4.4 Data availability

The cDNA sequence coding for pIgR from *T. bernacchii* has been desposited in the GenBank database (https://www.ncbi.nlm.nih.gov/genbank/) under the accession number MZ540772. The nucleotide sequences from the other species used for molecular analysis are reported in Table S3.

pIgR predicted transcripts from *S. lucioperca* (v. SLUC_FBN_1.2) [40]; *P. fluviatilis* (v. GENO_Pfluv_1.0) [41], *P. flavescens* (v. PFLA_1.0) [42], *E. spectabile* (v. UIUC_Espe_1.0) [43], *E. cragini* (v. CSU_Ecrag_1.0) [44], *E. lanceolatus* (v. ASM528154v1) [45], *P. leopardus* (v. YSFRI_Pleo_2.0) [46], *P. pungitius* (v. NSP_V7) [47], *A. ocellatus* (v. GSC_Weel_1.0) [48] and *G. aculeatus* (v. GAculeatus_UGA_version5) [49] were retrieved from research articles that first reported them.

pIgR transcripts from the Antarctic species *D. eleginoides* [50], *N. coriiceps* [51] *H. antarcticus* [52] and *C. hamatus* [53], and from the serranoid species *E. coioides* [10] were retrieved from transcriptome shotgun assemblies, whereas for the Antarctic species *D. mawsoni* [54], *C. myersi* [55] and *C. aceratus* [56] from partial genome assemblies.

4.5 Deduced amino acid sequence analyses

Preprints (www.preprints.org) | NOT PEER-REVIEWED | Posted: 17 February 2022 doi:10.20944/preprints202202.0211.v1

The amino acid sequences were deduced from nucleotide sequence using the ExPASy Translate Tool (https://web.expasy.org/translate/).

The amino acid composition was analyzed using the ProtParam [57] and Pep-Calc (www.pepcalc.com) tools.

The transmembrane-spanning regions and their orientation were predicted by using the TMpred tool [58].

The presence of the signal peptide was determined by using the SignalP-6.0 Sever tool [59]. Multiple sequence alignments were performed with Clustal Omega (https://www.ebi.ac.uk/Tools/msa/clustalo/) [60] and the out alignments were obtained in ClustalW format [61]. A distance-based tree of the D1 sequences Clustal Omega out alignment was reconstructed and analysed by iTOL program (https://itol.embl.de/) [62].

Sequons and putative N-glycosylation sites were identified using the NetNGlyc 4.0 Server [63].

A 3D molecular model was built for the *T. bernacchii* pIgR ectodomain using the Phyre2 tool (http://www.sbg.bio.ic.ac.uk/phyre/html/) [64]: 97% of the amino acid residues was modeled at 100% confidence using the 5f1s PDBe template (*Oncorhyncus mykiss* pIgR).

A Phyre molecular model was also built for the transmembrane domain. The highest confidence was 69% with 6rx4 PDBe template. The obtained PDB models were analyzed by the molecular graphics program YASARA [65] (www.yasara.org).

4.6 Expression analysis of pIgR by qReal-time PCR

Total RNA was extracted, using SV Total RNA Isolation System kit (Promega), from 150 mg each of anterior, middle and posterior gut, liver, gills, head kidney and muscle collected from three *T. bernacchii* specimens. Quantitative PCR-based expression analysis was performed on *T. bernacchii* cDNA using the Light Cycler 480 (Roche). The reaction consisted of 2 µl of cDNA diluted 1:10 and mixed with 5 µl of PowerUp™ SYBR™ Green Master Mix 2X (Applied Byosystem™) in a final volume of 10 µl with a final concentration of 0.3 µM of each primer, according to the manufacturer's instructions. TbrtpIgRFwd and TbrtpIgRRev are primers designed on the D1 and D2 domains respectively for the amplification of products from *T. bernacchii pIgR* (Table S2). qPCR was performed three times and samples, including DEPC water as negative control, were run in duplicate each time. The PCR amplification conditions were: 95 °C for 2 min, followed by 40 cycles of 95 °C (15 s), 60 °C (15 s), 72 °C (1 m). In order to assess the amplification specificity and the absence of primer dimers, a final dissociation step was run to generate a melting curve. In all melting curve analyses, single specific peaks were observed. The relative expression of *pIgR* was determined using β-actin as housekeeper gene (Table S2) and muscle as a calibrator with the $2^{-\Delta\Delta Cq}$ method.

Comparison between mucosal and lymphoid tissues was performed using two-tailed paired Student's t-tests adjusted by Bonferroni *post hoc* test. Data are presented as means ± standard deviation. p values <0.05 are considered as statistically significant, and shown as * $p<0.05$, ** $p<0.01$, *** $p<0.001$.

Preprints (www.preprints.org) | NOT PEER-REVIEWED | Posted: 17 February 2022 doi:10.20944/preprints202202.0211.v1

4.7 In situ hybridization (ISH)

4.7.1 Synthesis of RNA probes

Cells from gills of *T. bernacchii* were obtained by tissue teasing and suspended in Tripure (Roche). Total RNA was isolated and resuspended in DEPC-treated water. For reverse transcription, the BioScript RNase H minus (Bioline) enzyme was employed, using 1 µg of total RNA and 0.5 µg of random primers [pd(N)6]. Specific PCR primers (Table S4) were designed to amplify a 419 nt product corresponding to *T. bernacchii* pIgR sequence.
Reactions were carried out in an Eppendorf Mastercycler personal (Milano, Italy). The cycling conditions were: 1 cycle of 94°C for 5 min, 35 cycles of 94 °C for 45 s, 52°C for 45 s, 72°C for 45 s, followed by 1 cycle of 72°C for 10 min. The resulting DNA was purified using the QIAquick Gel Extraction Kit (QIAgen), inserted into the pGEM-T Easy vector (Promega) and transfected into competent JM109 *E. coli* cells. Plasmid DNA from three independent clones was purified using the Wizard Plus SV Minipreps DNA Purification System (Promega) and sequenced using Eurofins Genomic Sequencing Services. Sequence similarity searching was carried out using the BLAST program. Selected plasmid clones were used as target in PCR reactions to synthesize the anti-sense and sense probes (see primers in Table S4). PCR conditions for anti-sense probe were: 1 cycle of 94 °C for 5 min, 35 cycles of 94 °C for 45 s, 54 °C for 45 s, 72 °C for 45 s, followed by 1 cycle of 72 °C for 10 min. The cycling protocol used for sense probe (the negative control of ISH experiments) was: 1 cycle of 94 °C for 5 min, 35 cycles of 94 °C for 45 s, 48 °C for 45 s, 72 °C for 45 s, followed by 1 cycle of 72 °C for 10 min. The PCR-products obtained were purified from agarose gel using QIAquick gel extraction kit (QIAgen) and used to synthesize DIG-labelled RNA probes with the DIG-RNA Labeling Kit (Roche).

4.7.2. Staining procedures

Posterior intestine and liver from adult specimens (N =3) were fixed overnight at room temperature (RT) in 4% paraformaldehyde in 0.01 M, pH 7.4 phosphate buffered saline (PBS), then dehydrated, embedded in paraffin wax and cut into 7µm-thick sections using a rotary microtome. Serial sections were collected on poly-Llysinecoated slides, air-dried overnight at 37 °C and stored at RT for subsequent investigation. After dewaxing in xilene and rehydration in graded ethanol series, sections were washed with DEPC water before proteinase K (Sigma-Aldrich) digestion. The concentration of proteinase K was titrated for posterior intestine and liver and the best results were obtained with 1 µg/ml. The digestion was stopped by immersion in cold DEPC water. Acetylation was performed by incubating sections in 0.25% acetic anhydride in 85 mM Tris-HCl buffer, containing 0.2% acetic acid and 0.02 M ethylenediaminetetraacetic acid (EDTA) for 10 min. Following rinses in DEPC water, sections were gradually dehydrated and incubated overnight at 45 °C with the probes (concentrations varying from 0.3 to 0.6 ng/ml) and the optimal one resulted 0.45 ng/ml. Subsequently, sections were washed with 2 x saline-sodium citrate (SSC)

 doi:10.20944/preprints202202.0211.v1

buffer at RT, then with 0.2 x SSC at 55 °C for 90 min and incubated for 30 min with 20 µg/ml RNAase A in 0.01M Tris-HCl containing 0.5MNaCl and 1mMEDTA. Sections were transferred for 1 h to Buffer 1 (0.1 M Tris containing0.15 M NaCl and 1% blocking reagent), then for 30 min to Buffer 2 (0.1 M Tris containing 0.15 M NaCl, 0.5% BSA and 0.3% Triton X- 100). Then, sections were incubated for 2 h at RT with alkaline phosphatase-conjugated anti-digoxigenin antibody (Fab fragment; Roche Diagnostic, Germany) diluted 1:1000 in Buffer 2, then washed with 0.1 M Tris containing 0.15 M NaCl and Buffer 3 (0.1 M Tris containing 0.1 M NaCl and 50 mM $MgCl_2$). Following staining with nitro blue tetrazoliumchloride and 5-bromo-4-chloro-3-indolyl-phosphate (Roche Diagnostic, Germany), sections were mounted with Aquatex, aqueous mounting agent for microscopy (Merck, USA) and examined under bright-field illumination. Images were acquired by a Zeiss Axioskop 2 plus a microscope equipped with the Axiocam MRC camera and the Axiovision software (Carl Zeiss, Oberkochen, Germany).

Supplementary Materials: The following are available online at www.mdpi.com/xxx/s1, **Figure S1.** 3D molecular model of the transmembrane helix of *T. bernacchii* pIgR built with the Phyre2 tool (http://www.sbg.bio.ic.ac.uk/phyre/html/). **Figure S2.** Multiple alignment of the deduced amino acid sequences of pIgRs. **Figure S3.** Detail of R60, K103, E114, and N161 residues in the 3D molecular model built for the secretory component of *T. bernacchii* pIgR. **Table S1**. Amino acid composition of *T. bernacchii* pIgR and the respective regions SC (Secretory Component), EMPD (Extra-cellular proximal domain), TM (Transmembrane domain), Cyt (Cytoplasmic tail). **Table S2**. List of primers used in PCR experiments. **Table S3.** List of perciform suborders and respective species investigated for *pIgR* genomic and transcript sequences available.
Table S4. Specific primers used for RT-PCR and sense and anti-sense probes.

Author Contributions: Conceptualization, A.A., S.P. and M.R.C.; validation, A.A., S.P. and U.O.; formal analysis, A.A., L.G., S.G. and U.O.; investigation, A.A., S.P, L.G. and S.G..; resources, S.P. and M.R.C.; writing—original draft preparation, A.A., U.O. and M.R.C.; writing—review and editing, A.A., S.P., S.G., U.O. and M.R.C.; visualization, A.A., S.P., L.G., U.O. and M.R.C.; project administration, S.P. and M.R.C.; funding acquisition, S.P. and M.R.C. All authors have read and agreed to the published version of the manuscript.

Funding: This research was funded by the Italian National Program for Research in Antarctica, grant number PNRA18_00077.

Institutional Review Board Statement: The study was conducted according to the "Protocol on environmental protection to the Antarctic Treaty" Annex V.

Informed Consent Statement: Not applicable.

Data Availability Statement: The data presented in this study are available in the Material and Methods Section, the Paragraph 4.4.

Acknowledgments: We are grateful to Dr. Ennio Cocca (IBBR, CNR, Naples, Italy) and Dr. Salvatore Fioriniello (IGB Buzzati-Traverso, CNR, Naples, Italy) for useful discussion and suggestions.

Conflicts of Interest: The authors declare no conflict of interest.

 doi:10.20944/preprints202202.0211.v1

References

1. Akula, S.; Mohammadamin, S.; Hellman, L. Fc receptors for immunoglobulins and their appearance during vertebrate evolution. *PLoS One.* **2014**, *9*, e96903, doi: 10.1371/journal.pone.0096903.
2. Kaetzel, C. S. Coevolution of mucosal immunoglobulins and the polymeric immunoglobulin receptor: evidence that the commensal microbiota provided the driving force. ISRN Immunology. **2014**, e541537, doi:10.1155/2014/541537.
3. Oreste, U.; Ametrano, A.; Coscia, M. R. On origin and evolution of the antibody molecule. *Biology.* **2021**, *10*, 140, doi:10.3390/biology10020140.
4. Mostov, K.E.; Friedlander, M.; Blobel, G. The Receptor for Transepithelial Transport of IgA and IgM Contains Multiple Immunoglobulin-like Domains. *Nature.* **1984**, *308*, 37–43, doi:10.1038/308037a0.
5. Kulseth, M.A.; Krajci, P.; Myklebost, O.; Rogne, S. Cloning and characterization of two forms of bovine polymeric immunoglobulin receptor cDNA. *DNA Cell Biol.* **1995**, *14*, 251–256, doi:10.1089/dna.1995.14.251.
6. Kuhn, L.C.; Kocher, H.P.; Hanly, W.C.; Cook, L.; Jaton, J.C.; Kraehenbuhl, J.P. Structural and genetic heterogeneity of the receptor mediating translocation of immunoglobulin A dimer antibodies across epithelia in the rabbit. *J Biol Chem.* **1983**, *258*, 6653–6659, doi:10.1016/S0021-9258(18)32462-1.
7. Wieland, W.H.; Orzaez, D.; Lammers, A.; Parmentier, H.K.; Verstegen, M.W.; Schots, A. A functional polymeric immunoglobulin receptor in chicken (*Gallus gallus*) indicates ancient role of secretory IgA in mucosal immunity. *Biochem J.* **2004**, *380*, 669-676, doi:10.1042/bj20040200.
8. Magadán-Mompo', S.; Sánchez-Espinel, C.; Gambón-Deza, F. IgH loci of American alligator and saltwater crocodile shed light on IgA evolution. *Immunogenet.* **2013**, *65*, 531‑541, doi:10.1007/s00251-013-0692-y.
9. Braathen, R.; Hohman, V.S.; Brandtzaeg, P.; Johansen, F.-E. Secretory antibody formation: conserved binding interactions between J chain and polymeric Ig receptor from humans and amphibians. *J Immunol.* **2007**, *178*, 1589–1597, doi:10.4049/jimmunol.178.3.1589.
10. Feng, L.-N.; Lu, D.-Q.; Bei, J.-X.; Chen, J.-L.; Liu, Y.; Zhang, Y.; Liu, X.-C.; Meng, Z.-N.; Wang, L.; Lin, H.-R. Molecular cloning and functional analysis of polymeric immunoglobulin receptor gene in orange-spotted grouper (*Epinephelus coioides*). *Comp Biochem Physiol B, Biochem Mol Biol*. **2009**, *154*, 282–289, doi:10.1016/j.cbpb.2009.07.003.
11. Salinas, I.; Fernández-Montero, Á.; Ding, Y.; Sunyer, J.O. Mucosal immunoglobulins of teleost fish: A decade of advances. *Dev Comp Immunol.* **2021**, *121*, 104079, doi:10.1016/j.dci.2021.104079.
12. Hohman, V.S.; Stewart, S.E.; Rumfelt, L.L.; Greenberg, A.S.; Avila, D.W.; Flajnik, M. F.; Steiner, L.A. J chain in the nurse shark: implications for function in a lower vertebrate. *J Immunol.* **2003**, *170*, 6016 – 6023, doi:10.4049/jimmunol.170.12.6016.
13. Kaetzel, C. S. The polymeric immunoglobulin receptor: bridging innate and adaptive immune responses at mucosal surfaces. *Immunol Rev.* **2005**, *206*, 83–99, doi:10.1111/j.0105-2896.2005.00278.x.

14. Kong, X.; Wang, L.; Pei, C.; Zhang, J.; Zhao, X.; Li, L. Comparison of polymeric immunoglobulin receptor between fish and mammals. *Vet Immunol and Immunopath.* **2018**, *202*, 63–69, doi:10.1016/j.vetimm.2018.06.002.

15. Kortum, A.N.; Rodriguez-Nunez, I.; Yang, J.; Shim, J.; Runft, D.; O'Driscoll, M.L.; Haire, R.N.; Cannon, J.P.; Turner, P.M.; Litman, R. T.; et al. Differential expression and ligand binding indicate alternative functions for zebrafish polymeric immunoglobulin receptor (PIgR) and a family of pigr-like (PIGRL) proteins. *Immunogenet.* **2014**, *66*, 267–279, doi:10.1007/s00251-014-0759-4.

16. Near, T.J.; Ghezelayagh, A.; Ojeda, F.P.; Dornburg, A. Recent diversification in an ancient lineage of notothenioid fishes (Bovichtus: Notothenioidei). *Polar Biol.* **2019**, *42*, 943–952, doi:10.1007/s00300-019-02489-1.

17. Eastman, J.T. Antarctic fish biology: evolution in a unique environment vol.30, *Academic Press, San Diego*, **1993**, 59-60.

18. Near, T.J.; Dornburg, A.; Harrington, R.C.; Oliveira, C.; Pietsch, T.W.; Thacker, C.E.; Satoh, T.P.; Katayama, E.; Wainwright, P.C.; Eastman, J.T.; et al. Identification of the notothenioid sister lineage illuminates the biogeographic history of an Antarctic adaptive radiation. *BMC Evol Biol.* **2015**, *15*, 109, doi:10.1186/s12862-015-0362-9.

19. Coscia, M. R.; Varriale, S.; Giacomelli, S.; Oreste, U. Antarctic teleost immunoglobulins: more extreme, more interesting. *Fish Shellfish Immunol*. **2011**, *31*, 688–696, doi:10.1016/j.fsi.2010.10.018.

20. Giacomelli, S.; Buonocore, F.; Albanese, F.; Scapigliati, G.; Gerdol, M.; Oreste, U.; Coscia, M. R. New insights into evolution of IgT genes coming from Antarctic teleosts. *Mar Genomics.* **2015**, *24*, 55–68, doi:10.1016/j.margen.2015.06.009.

21. Ametrano, A.; Gerdol, M.; Vitale, M.; Greco, S.; Oreste, U.; Coscia, M.R. The evolutionary puzzle solution for the origins of the partial loss of the Cτ2 exon in notothenioid fishes. *Fish Shellfish Immunol.* **2021**, *116*, 124–139, doi:10.1016/j.fsi.2021.05.015.

22. Abelli, L.; Coscia, M.R.; De Santis, A.; Zeni, C.; Oreste, U. Evidence for hepato-biliary transport of immunoglobulin in the Antarctic teleost fish *Trematomus bernacchii*. *Devel Comp Immunol.* **2005**, *29*, 431–442, doi:10.1016/j.dci.2004.09.004.

23. Wei, H.; Wang, J.-Y. Role of polymeric immunoglobulin receptor in IgA and IgM transcytosis. *Int J Mol Sci.* **2021**, *22*, 2284, doi:10.3390/ijms22052284.

24. Hamuro, K.; Suetake, H.; Saha, N.R.; Kikuchi, K.; Suzuki, Y. A teleost polymeric Ig receptor exhibiting two Ig-like domains transports tetrameric IgM into the skin. *J Immunol.* **2007**, *178*, 5682–5689, doi:10.4049/jimmunol.178.9.5682.

25. Coscia, M.R.; Morea, V.; Tramontano, A.; Oreste, U. Analysis of a cDNA sequence encoding the immunoglobulin heavy chain of the Antarctic teleost *Trematomus bernacchii*. *Fish Shellfish Immunol.* **2000**, *10*, 343–357, doi:10.1006/fsim.1999.0244.

26. Pei, C.; Sun, X.; Zhang, Y.; Li, L.; Gao, Y.; Wang, L.; Kong, X. Molecular cloning, expression analyses of polymeric immunoglobulin receptor gene and its variants in grass carp (*Ctenopharyngodon Idellus*) and binding

assay of the recombinant immunoglobulin-like domains. *Fish Shellfish Immunol.* **2019**, *88*, 472–479, doi:10.1016/j.fsi.2019.03.024.

27. Rombout, J.; Vandertuin, S.; Yang, G.; Schopman, N.; Mroczek, A.; Hermsen, T.; Tavernethiele, J. Expression of the polymeric immunoglobulin receptor (PIgR) in mucosal tissues of common carp (*Cyprinus carpio l.*). *Fish Shellfish Immunol.* **2008**, *24*, 620–628, doi:10.1016/j.fsi.2008.01.016.

28. Tadiso, T. M.; Sharma, A.; Hordvik, I. Analysis of Polymeric Immunoglobulin Receptor- and CD300-like Molecules from Atlantic Salmon. *Mol Immunol.* **2011**, *49*, 462–473, doi:10.1016/j.molimm.2011.09.013.

29. Xu, Z.; Parra, D.; Gómez, D.; Salinas, I.; Zhang, Y.-A.; Jørgensen, L. von G.; Heinecke, R. D.; Buchmann, K.; LaPatra, S.; Sunyer, J. O. Teleost skin, an ancient mucosal surface that elicits gut-like immune responses. *PNAS.* **2013a**, *110*, 13097–13102, doi:10.1073/pnas.1304319110.

30. Deaton, A. M.; Bird, A. CpG Islands and the Regulation of Transcription. *Genes Dev.* **2011**, *25* (10), 1010–1022, doi:10.1101/gad.2037511.

31. Varriale, A.; Bernardi, G. DNA methylation and body temperature in fishes. *Gene.* **2006**, *385*, 111–121, doi:10.1016/j.gene.2006.05.031.

32. Palm, H. W. Ecology of Pseudoterranova Decipiens (Krabbe, 1878) (Nematoda: Anisakidae) from Antarctic Waters. *Parasitol Res.* **1999**, *85*, 638–646, doi:10.1007/s004360050608.

33. Orecchia, P.; Mattiucci, S.; D'Amelio, S.; Paggi, L.; Plötz, J.; Cianchi, R.; Nascetti, G.; Arduino, P.; Bullini, L. Two new members in the Contracaecum Osculatum Complex (Nematoda, Ascaridoidea) from the Antarctic. *Int J Parasitol.* **1994**, 24, 367–377, doi:10.1016/0020-7519(94)90084-1.

34. Sheng, X.; Qian, X.; Tang, X.; Xing, J.; Zhan, W. Polymeric immunoglobulin receptor mediates immune excretion of mucosal igm–antigen complexes across intestinal epithelium in flounder (*Paralichthys olivaceus*). *Front Immunol*. **2018**, *9*, doi:10.3389/fimmu.2018.01562.

35. Salinas, I.; Parra, D. 6 - Fish mucosal immunity: intestine. In *Mucosal Health in Aquaculture*; Beck, B. H., Peatman, E., Eds.; Academic Press: San Diego, **2015**; pp 135–170, doi:10.1016/j.dci.2021.104079.

36. Brandl, K.; Kumar, V.; Eckmann, L. Gut-liver axis at the frontier of host-microbial interactions. *Am J Physiol-Gastr L.* **2017**, *312*, G413–G419, doi:10.1152/ajpgi.00361.2016.

37. Xu, G.; Zhan, W.; Ding, B.; Sheng, X. Molecular cloning and expression analysis of polymeric immunoglobulin receptor in flounder (*Paralichthys olivaceus*). *Fish Shellfish Immunol.* **2013**b, *35*, 653–660, doi:10.1016/j.fsi.2013.05.024.

38. Zhang, Y.-A.; Salinas, I.; Li, J.; Parra, D.; Bjork, S.; Xu, Z.; LaPatra, S. E.; Bartholomew, J.; Sunyer, J. O. IgT, a primitive immunoglobulin class specialized in mucosal immunity. *Nat Immunol.* **2010**, *11*, 827–835, doi:10.1038/ni.1913.

39. Yu, Y.; Liu, Y.; Li, H.; Dong, S.; Wang, Q.; Huang, Z.; Kong, W.; Zhang, X.; Xu, Y.; Chen, X. et al. Polymeric immunoglobulin receptor in dojo loach (*Misgurnus anguillicaudatus*): molecular characterization and expression

analysis in response to bacterial and parasitic challenge. *Fish Shellfish Immunol*. **2018**, *73*, 175–184, doi:10.1016/j.fsi.2017.12.019.

40. Nguinkal, J.A.; Brunner, R.M.; Verleih, M.; Rebl, A.; Ríos-Pérez, L. de los; Schäfer, N.; Hadlich, F.; Stüeken, M.; Wittenburg, D.; Goldammer, T. The first highly contiguous genome assembly of pikeperch (*Sander lucioperca*), an emerging aquaculture species in Europe. *Genes*. **2019**, *10*, 708, doi:10.3390/genes10090708.

41. Roques, C.; Zahm, M.; Cabau, C.; Klopp, C.; Bouchez, O.; Donnadieu, C.; Kuhl, H.; Gislard, M.; Guendouz, S.; Journot, L. et al. A chromosome-scale genome assembly of the European perch, *Perca fluviatilis*. *Submitted (JUN-2019) to the EMBL/GenBank/DDBJ databases.*

42. Feron, R.; Morvezen, R.; Bestin, A.; Haffray, P.; Klopp, C.; Zahm, M.; Cabau, C.; Roques, C.; Donnadieu, C.; Bouchez, O. et al. A chromosome-scale genome assembly of the yellow perch, *Perca flavescens*. *Submitted (JAN-2019) to the EMBL/GenBank/DDBJ databases.*

43. Moran, R.L.; Catchen, J.M.; Fuller, R.C. A chromosome-level genome assembly, high-density linkage maps, and genome scans reveal the genomic architecture of hybrid incompatibilities underlying speciation via character displacement in darters (Percidae: Etheostominae). *Submitted (AUG-2019) to the EMBL/GenBank/DDBJ databases.*

44. Reid, B.N.; Moran, R.L.; Kopack, C.J.; Fitzpatrick, S. W. Rapture-Ready Darters: Choice of reference genome and genotyping method (whole-genome or sequence capture) influence population genomic inference in Etheostoma. *Mol Ecol Resour.* **2021**, *21*, 404–420, doi:10.1111/1755-0998.13275.

45. Zhou, Q.; Gao, H.; Zhang, Y.; Fan, G.; Xu, H.; Zhai, J.; Xu, W.; Chen, Z.; Zhang, H.; Liu, S.; et al. A chromosome-level genomea of the giant grouper (*Epinephelus Lanceolatus*) provides insights into its innate immunity and rapid growth. *Mol Ecol Resour.* **2019**, *19,* 1322–1332, doi:10.1111/1755-0998.13048.

46. Zhou, Q.; Guo, X.; Huang, Y.; Gao, H.; Xu, H.; Liu, S.; Zheng, W.; Zhang, T.; Tian, C.; Zhu, C.; et al. De novo sequencing and chromosomal-scale genome assembly of leopard coral grouper, Plectropomus Leopardus. *Mol Ecol Resour.* **2020**, *20*, 1403–1413, doi:10.1111/1755-0998.13207.

47. Varadharajan, S. *Pungitius pungitius* genome assembly, contig: LG2, whole genome shotgun sequence. *Submitted (OCT-2019) to the EMBL/GenBank/DDBJ databases.*

48. Culibrk, L.; Leelakumari, S.; Taylor, G.A.; Tse, K.; Cheng, D.; Chuah, E.; Kirk, H.; Pandoh, P.; Troussard, A.; Zhao, Y.; et al. The genome of the wolf eel (*Anarrhichthys ocellatus*). *Submitted (JAN-2019) to the EMBL/GenBank/DDBJ databases.*

49. Nath, S.; Shaw, D.E.; White, M. A. Improved contiguity of the threespine stickleback genome using long-read sequencing. *G3*. **2021**, *11*, jkab007, doi:10.1093/g3journal/jkab007.

50. Touma, J.; García, K.K.; Bravo, S.; Leiva, F.; Moya, J.; Vargas-Chacoff, L.; Reyes, A.; Vidal, R. De novo assembly and characterization of patagonian toothfish transcriptome and develop of EST-SSR markers for population genetics. *Front in Mar Sci*. **2019**, *6*, 720, doi:10.3389/fmars.2019.00720.

51. Shin, S.C.; Kim, S. J.; Lee, J.K.; Ahn, D.H.; Kim, M.G.; Lee, H.; Lee, J.; Kim, B.-K.; Park, H. Transcriptomics and comparative analysis of three Antarctic notothenioid fishes. *PLoS One.* **2012**, 7, e43762, doi:10.1371/journal.pone.0043762.

52. York, J. M.; Zakon, H. H. Evolution of transient receptor potential (TRP) ion channels in Antarctic Fishes (Cryonotothenioidea) and identification of putative thermosensors. *Genome Biol Evol*. **2022**, 14, evac009, doi:10.1093/gbe/evac009.

53. Song, W.; Li, L.; Huang, H.; Jiang, K.; Zhang, F.; Wang, L.; Zhao, M.; Ma, L. Tissue-based transcriptomics of *Chionodraco hamatus*: sequencing, de novo assembly, annotation and Marker discovery. *J Fish Biol.* **2019**, *94*, 251–260, doi:10.1111/jfb.13882.

54. Lee, S. J.; Kim, J.-H.; Jo, E.; Choi, E.; Kim, J.; Choi, S.-G.; Chung, S.; Kim, H.-W.; Park, H. Chromosomal assembly of the Antarctic toothfish (*Dissostichus mawsoni*) genome using third-generation DNA sequencing and Hi-C technology. *Zool Res*. **2021**, *42*, 124–129, doi:10.24272/j.issn.2095-8137.2020.264.

55. Bargelloni, L.; Babbucci, M.; Ferraresso, S.; Papetti, C.; Vitulo, N.; Carraro, R.; Pauletto, M.; Santovito, G.; Lucassen, M.; Mark, F. C.; et al. Draft genome assembly and transcriptome data of the icefish *Chionodraco myersi* reveal the key role of mitochondria for a life without hemoglobin at subzero temperatures. *Commun Biol*. **2019**, *2*, 1–11, doi:10.1038/s42003-019-0685-y.

56. Jakobsen, S.K.; Tørresen, K.O., Boessenkool, S.; Malmstrøm, M.; Star, B.; Jakobsen, S.K.; Riiser, S.E. The *Chaenocephalus aceratus* whole genome shotgun project. *Submitted (MAR-2018) to the EMBL/GenBank/DDBJ database.*

57. Gasteiger, E.; Hoogland, C.; Gattiker, A.; Duvaud, S.; Wilkins, M. R.; Appel, R. D.; Bairoch, A. Protein identification and analysis tools on the ExPASy Server. In The Proteomics Protocols Handbook; Walker, J. M., Ed.; Humana Press: Totowa, NJ, **2005**, 571–607.

58. Cuthbertson, J. M.; Doyle, D. A.; Sansom, M. S. P. Transmembrane helix prediction: A comparative evaluation and analysis. *Protein Eng Des Sel.* **2005**, *18*, 295–308, doi:10.1093/protein/gzi032.

59. Teufel, F.; Armenteros, J. J. A.; Johansen, A. R.; Gíslason, M. H.; Pihl, S. I.; Tsirigos, K. D.; Winther, O.; Brunak, S.; Heijne, G. von; Nielsen, H. SignalP 6.0 achieves signal peptide prediction across all types using protein language models. *bioRxiv.* **2021**, 447770.

60. Sievers, F.; Higgins, D. G. Clustal Omega, accurate alignment of very large numbers of sequences. In Multiple Sequence Alignment Methods; Russell, D. J., Ed.; Methods in Molecular Biology; Humana Press: Totowa, NJ. **2014**, 105–116.

61. Thompson, J.D.; Higgins, D.G.; Gibson, T.J. CLUSTAL W: improving the sensitivity of progressive multiple sequence alignment through sequence weighting, position-specific gap penalties and weight matrix choice. *Nucleic Acids Res*. **1994**, *22*, 4673–4680, doi:10.1093/nar/22.22.4673.

62. Letunic, I.; Bork, P. Interactive tree of life (ITOL): An online tool for phylogenetic tree display and Annotation. *Bioinformatics*. **2007**, *23*, 127–128, doi:10.1093/bioinformatics/btl529.

 doi:10.20944/preprints202202.0211.v1

63. Gupta, R.; Brunak, S. Prediction of glycosylation across the human proteome and the correlation to protein function. *Pac Symp Biocomput.* **2002**, 310-322.

64. Kelley, L.A.; Mezulis, S.; Yates, C.M.; Wass, M.N.; Sternberg, M.J.E. The Phyre2 web portal for protein modeling, prediction and analysis. *Nat Protoc*. **2015**, *10*, 845–858, doi:10.1038/nprot.2015.053.

65. Krieger, E.; Vriend, G. Models@Home: distributed computing in bioinformatics Using a Screensaver Based Approach. *Bioinformatics* 2002, 18 (2), 315–318, doi:10.1093/bioinformatics/18.2.315.